Influence of the grain size on deleterious phase precipitation in superduplex stainless steel UNS S32750

J.M. Pardal[a], S.S.M. Tavares[a,*], M. Cindra Fonseca[a], J.A. de Souza[a], R.R.A. Côrte[a], H.F.G. de Abreu[b]

[a]Universidade Federal Fluminense, Departamento de Engenharia Mecânica, Rua Passo da Pátria, 156-CEP 24210-240, Niterói/Brazil
[b]Universidade Federal do Ceará, Departamento de Engenharia Metalúgica e de Materiais, Campus do Pici Bl. 702, Fortaleza, CE, CEP 60.455-760, Brazil

ARTICLE DATA

Article history:
Received 15 May 2008
Accepted 27 August 2008

Keywords:
Superduplex stainless steel
Phase quantification
Mechanical properties
Corrosion resistance

ABSTRACT

In the present work, the effect of grain size on deleterious phase precipitation in a superduplex stainless steel was investigated. The materials studied were heat treated isothermally at 800 °C, 850 °C and 900 °C for times up to 120 min. Hardness tests, light optical microscopy, scanning electron microscopy and X-ray diffraction were carried out to detect sigma and other harmful precipitate phases. The ferritic and austenitic grain sizes in the solution treated condition of the two steels analyzed were measured by electron backscattered diffraction (EBSD). Cyclic polarization corrosion tests were performed to evaluate the effect of grain size on the corrosion resistance. The results presented show that the precipitation of deleterious phases such as χ, σ and γ_2, which can occur during welding and forming operations, is retarded by grain growth.

1. Introduction

Due to their high corrosion resistance and improved mechanical properties superduplex stainless steels (SDSS) are extensively used in petrochemical plants such as facilities in modern oil platforms and off-shore process equipment. Pipes, pumps, pressure vessels, separators and heat exchangers are some examples of these applications.

It is well established that the best mechanical and corrosion resistance properties of duplex and superduplex steels are found with a microstructure with approximately equal amounts of austenite and ferrite [1], and when other tertiary phases are not present. These phases, such as sigma (σ), chi (χ), secondary austenite (γ_2), chromium carbides and nitrides must be avoided due to their adverse effects on mechanical and corrosion resistance properties.

For instance, in duplex stainless steels, σ can be formed in the 600–1000 °C range. However, this interval is strongly dependent on the chemical composition of the alloy [2]. Sigma phase is considered the most dangerous because of its influence on toughness and corrosion resistance [3,4]. Chi is a Mo-rich phase which forms before σ phase. In fact, χ and σ provoke similar effects on the materials properties, but are not well distinguished by optical microcopy [5].

Nucleation and growth of deleterious phases has been studied by many authors [6–11]. Some findings that have been reported included:

- The formation of σ and χ occurs from the ferrite phase, due to its higher Cr and Mo concentrations, and also due to the higher diffusivities in this phase [6,8].
- γ/δ boundaries, austenitized δ/δ sub-grain boundaries and high energy δ/δ boundaries are, in this order, preferential sites for σ nucleation [6].
- Precipitation of $Cr_{23}C_6$ may occur before σ precipitation, delaying its formation in SDSS with higher carbon contents

* *Corresponding author*. Tel.: +55 21 2629 5584; fax: +55 21 2629 5368.
E-mail address: ssmtavares@terra.com.br (S.S.M. Tavares).

1044-5803/$ – see front matter © 2008 Elsevier Inc. All rights reserved.
doi:10.1016/j.matchar.2008.08.007

Table 1 – Characteristics of the as received steels

Material designation		Product form	Dimensions (mm)	Heat treatment	Standard
SD-A	UNS S32750 (fine grain)	Tube	Ø=273; t=9.5–15.88	Solution treatment	ASTM A 928
SD-B	UNS S32750 (coarse grain)	Bar	Ø=203.20	Solution treatment	ASTM A 479

Table 2 – Mechanical properties of materials analyzed

Material	$\sigma_{YS.}$ (MPa)	σ_{UTS} (MPa)	Elongation in 50 mm (%)
SD-A	608	879	33.5
SD-B	535	735	35.0

[6,8]. In duplex stainless steels with very low carbon (<0.02%, for instance) chromium carbide precipitation is improbable [6,10].

- σ is found to precipitate in association with γ_2 by a reaction $\delta \rightarrow \sigma + \gamma_2$. Secondary austenite may also nucleate alone at the δ/δ boundaries in elevated temperatures due to high diffusion in these boundaries; however, it can also nucleate in Cr_2N particles inside the ferrite grains. Finally, secondary austenite (γ_2), that refers to any austenite that forms upon re-heating, can also be formed by growth of the former austenite islands [11]. One of the characteristics of this phase is the low nitrogen content, which leads to a poorer corrosion resistance when compared to the former austenite [9].

In the present work the kinetics of precipitation of the deleterious phases were compared in two SDSS UNS S32750 steels with similar composition but quite different grain sizes. The objective was to evaluate the effect of grain size on the formation of deleterious phases in the SDSS UNS S32750.

2. Experimental

In this work, two superduplex stainless steels, grade UNS S32750, designated "SD-A" and "SD-B", were purchased in the solution treated condition. Table 1 shows the main characteristics of each material, Table 2 shows the tensile properties and Table 3 shows the chemical compositions. Grain sizes of each material were determined by electron backscattered diffraction (EBSD) using a scanning electron microscope (SEM) equipped with an Oxford 300 EBSD system. Samples were prepared by grinding and polishing with colloidal silica for 10 min.

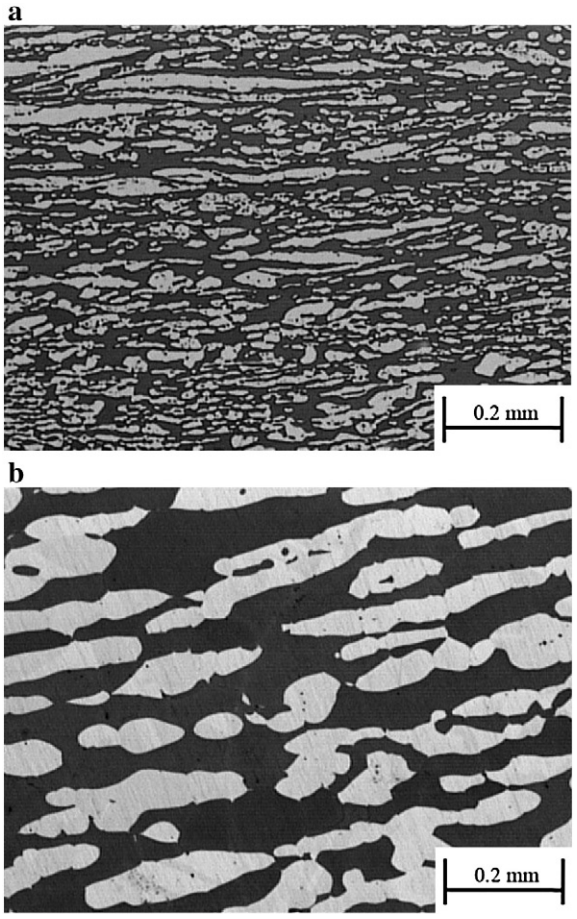

Fig. 1 – As received materials etched with Beraha's reagent: (a) SD-A; (b) SD-B.

Specimens with dimensions 15×10×5 mm of each material were cut for heat treatments and analysis. The samples were exposed at 800 °C, 850 °C, and 900 °C for 5, 15, 30, 45, 60, 90 and 120 min. After these treatments the Vickers hardnesses were determined in each condition with 30 kgf load. Volumetric fractions of austenite and ferrite in the as received materials, and deleterious phases in aged samples, were determined by quantitative metallography using Image Tool software [12]. The samples were prepared by grinding, polishing and etching by one of the following procedures:

- Electrolytic etching in a KOH solution (100 ml H_2O+15 g of potassium hydroxide), applying 3 V for 12 s. The parameters of this reagent were adjusted to reveal clearly σ phase and other deleterious phases, such as χ, γ_2, and eventually Cr_2N that precipitated in association with σ [5,13].

Table 3 – Chemical compositions of materials studied

Material	%wt. (%Fe=balance)										
	Cr	Ni	Mo	Mn	Si	N	Cu	W	C	P	S
SD-A	24.57	6.68	3.75	0.83	0.34	0.28	0.25	–	0.02	0.026	0.000
SD-B	24.80	6.75	3.79	0.78	0.54	0.27	0.10	0.04	0.019	0.026	0.001

- To reveal phases in the solution treated condition, immersion etching in Beraha's solution (100 ml H_2O + 20 ml HCl + 0.3–0.6 g of potassium metabisulfite) was used [14].

Characterization of deleterious phases was performed in a scanning electron microscope, JEOL 6460LV, for some of the heat treated samples.

X-ray diffraction was carried out on selected specimens. A Phillips X'PertPro diffractometer was used with CoKα (λ=0.17890 nm) without a monochromator. Other measured parameters were: voltage 40 kV, current 40 mA, angular interval (2θ) 35–110°, angular step 0.02° and counting time 3 s.

Anodic polarization tests were conducted at room temperature using a potentiostat-galvanostat Ominimetra® PG-40. The tests were conducted in a conventional three-electrode cell, with Pt foil as the auxiliary electrode, and a saturated calomel electrode (SCE) as the reference electrode. The working electrode was constructed using the SDSS samples embedded in epoxy resin, with a copper wire providing electrical contact. The tests were initiated after nearly steady-state open circuit potential (E_{oc}) had developed (about 30 min). After that, a potential sweep was applied in the anodic direction at 1 mVs^{-1} until a current density of 1 mA/cm^2 was reached. Prior to each experiment, the working electrodes were ground and polished with 0.1 μm alumina paste, degreased with alcohol and cleaned in water. The edges of the samples were protected to avoid crevice corrosion. The working solution was 1 M H_2SO_4 + 1 M NaCl. The corrosion behavior was evaluated by the absolute value of the pitting potential (E_p).

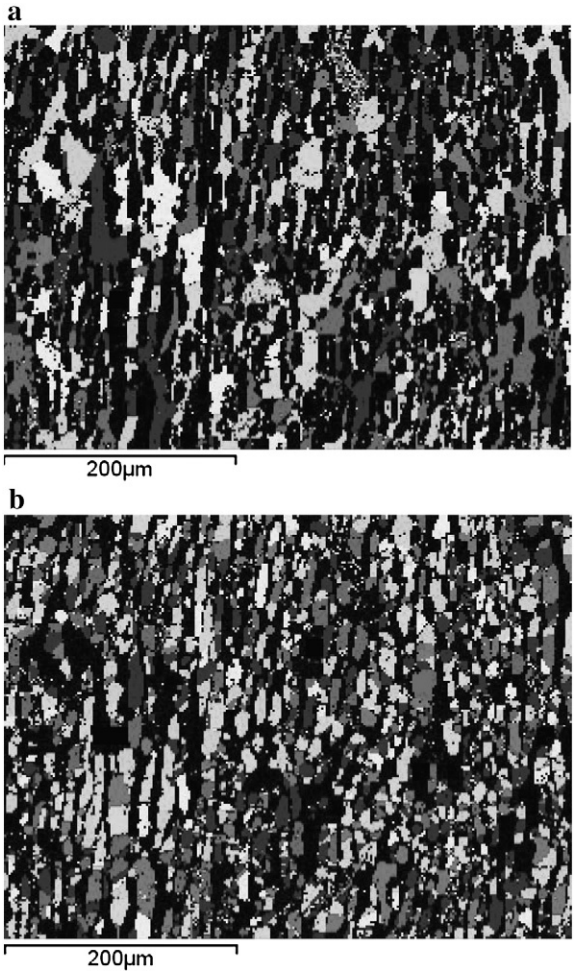

Fig. 2 – EBSD images from SD-A in the as received condition used to (a) ferrite grain size measurement and (b) austenite grains size measurement.

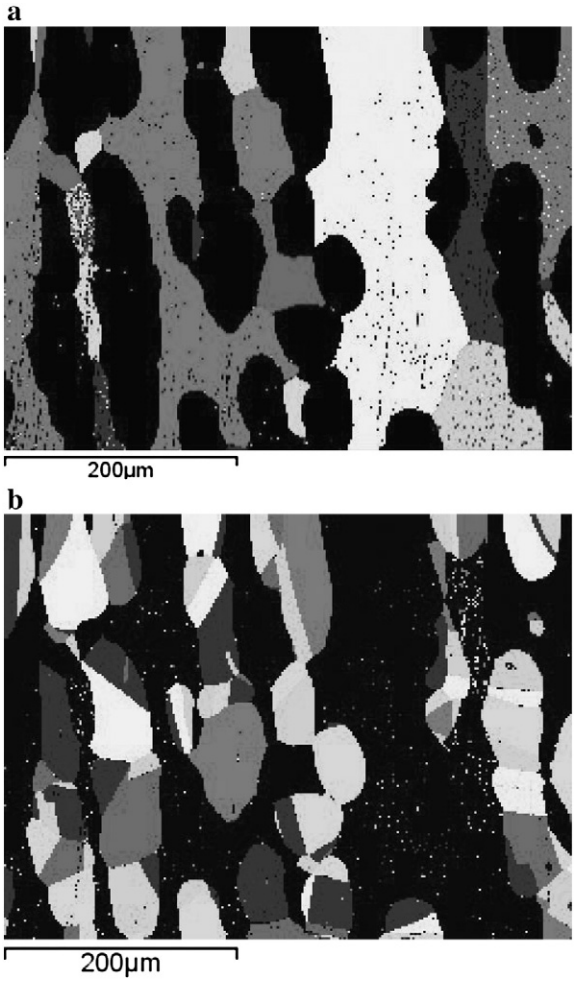

Fig. 3 – EBSD images from SD-B in the as received condition used to (a) ferrite grain size measurement and (b) austenite grains size measurement.

Table 4 – Percentages of ferrite and austenite and grain sizes in materials SD-A and SD-B as received

Material	Ferrite (δ)			Austenite (γ)		
	Amount (%)	Grain size		Amount (%)	Grain size	
		μm	ASTM no.		μm	ASTM no.
SD-A	55.05	29.42	12.1	44.95	24.75	12.3
SD-B	49.95	132.36	9.9	50.05	138.32	9.9

3. Results and Discussion

Fig. 1(a) and (b) show the as received microstructures of SD-A and SD-B. These images were taken with the same magnification. Beraha's etching does not reveal austenite and ferrite grain boundaries, but it's clear that material SD-A presents a much finer microstructure than SD-B. The measurement of grain sizes was performed by EBSD in the scanning electron microscope. Figures such as Fig. 2(a) and (b), from the same field, were used to determine the average ferrite and austenite grains, respectively, in SD-A. Similarly, Fig. 3(a) and (b) are for SD-B. Figs. 2(a) and 3(a) show austenite grains as black and ferrite grains with different tonalities in grayscale, where each tonality corresponds to a specific crystallographic orientation. Figs. 2(b) and 3(b) show ferrite as black and austenite in grayscale. The grains are distinguished by the tonality when the angular difference of orientation between them is greater than 15°. Considering this fact, the EBSD software calculates the average austenite and ferrite grain sizes. Table 4 shows the ferrite and austenite percentages and average grain sizes measured by EBSD by analysis of 10 different fields.

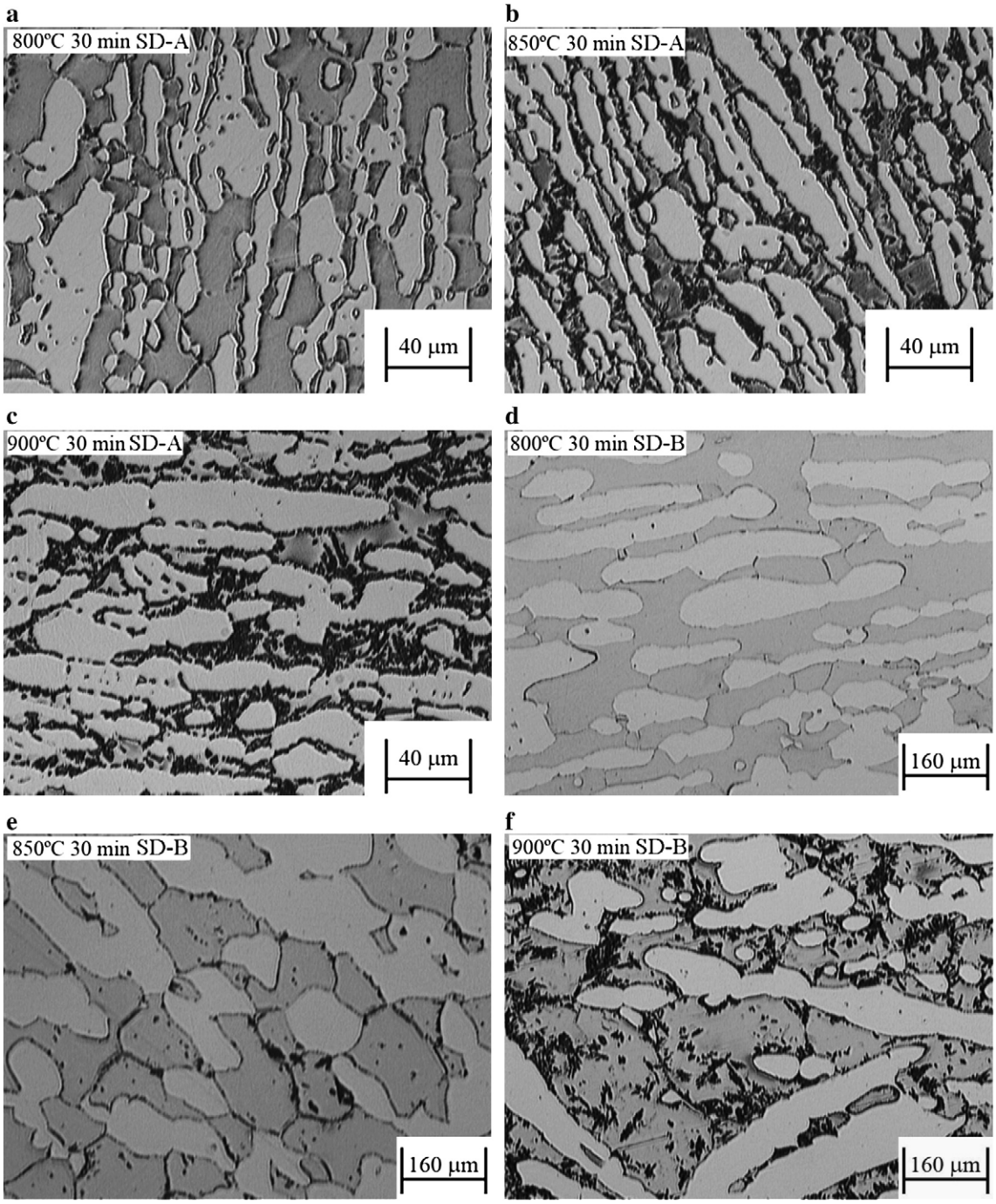

Fig. 4 – Light optical microscope images from samples aged for 30 min: (a) SD-A—800 °C; (b) SD-A—850 °C; (c) SD-A—900 °C; (d) SD-B—800 °C; (e) SD-B—850 °C; (f) SD-B—900 °C.

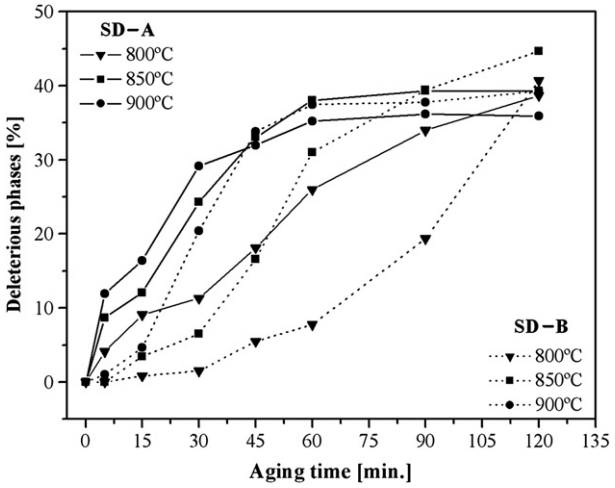

Fig. 5 – Amount of deleterious phases as function of aging time at 800 °C, 850 °C and 900 °C in SD-A and SD-B.

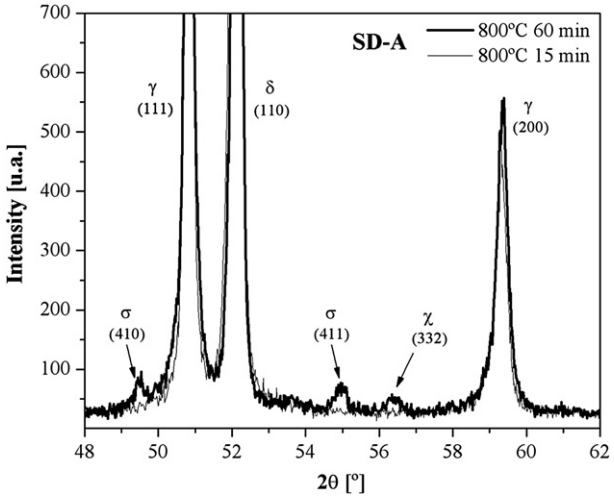

Fig. 7 – X-ray diffractograms of samples SD-A aged at 800 °C for 15 min and 60 min.

Fig. 4(a–f) show the light optical microscope (LOM) images of specimens of SD-A and SD-B aged at 800, 850 and 900 °C for 30 min. The electrolytic etching with the KOH solution reveals deleterious phases as black regions which can be quantified by image analysis. Fig. 5 shows the percentage of the deleterious phases as a function of aging time at 800 °C, 850 °C and 900 °C for materials SD-A and SD-B. The quantification in each condition was performed by analyzing 20 fields using different magnifications.

The differentiation between the deleterious phases may be obtained by careful examination in a scanning electron microscope (Fig. 6(a) and (b)). The χ phase corresponds to the light particles precipitated at the grain boundaries, while σ phase are gray particles. Black regions near σ and χ are chromium and molybdenum-depleted matrix grains, corresponding probably to γ_2 particles.

Fig. 7 shows the X-ray diffractograms of SD-A aged at 800 °C for 15 and 60 min. At these conditions, concentrations of 9.1% and 26.0% of the deleterious phases were determined by image analysis. Diffractograms of material SD-B aged at 800 °C for 60 min (not shown) presents almost imperceptible σ and χ peaks. Small amounts of χ and σ are not detected by X-ray diffraction due to overlap between χ and σ peaks with δ and, mainly, γ reflections, among other factors. A similar

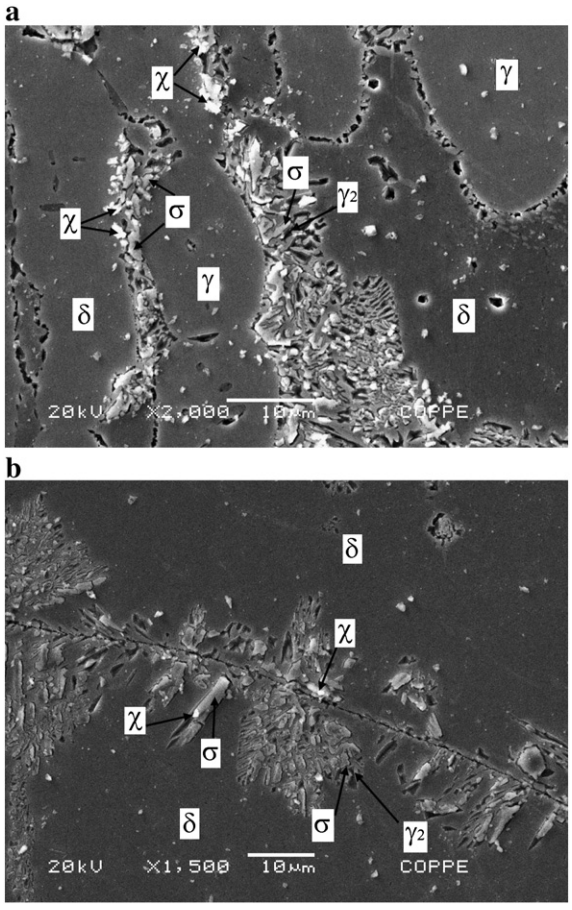

Fig. 6 – SEM images from samples treated at 800 °C for 60 min: (a) SD-A and (b) SD-B.

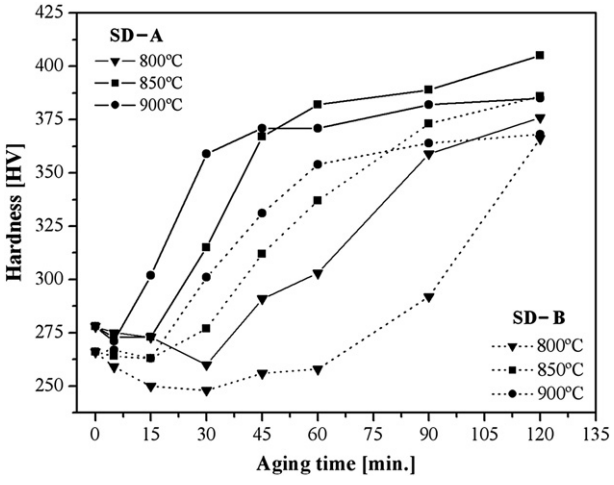

Fig. 8 – Hardness against aging time at 800 °C, 850 °C and 900 °C in SD-A and SD-B.

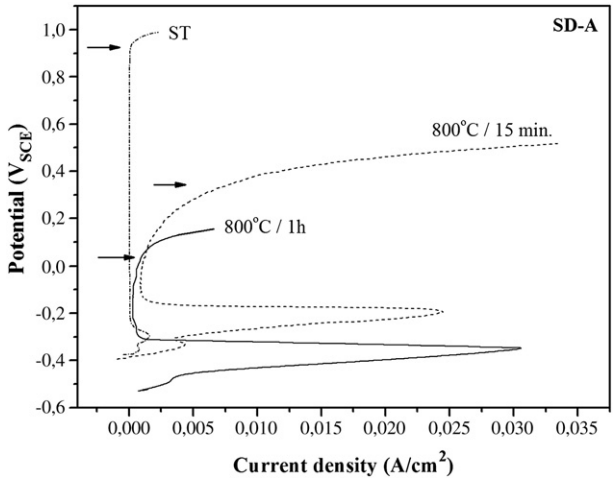

Fig. 9 – Anodic polarization curves from SD-A samples: as received (solution treated); 800 °C/60 min and 800 °C/1 h.

conclusion was obtained by Kim et al. [15]. Nevertheless, the diffractogram of a specimen aged at 800 °C for 60 min shows clearly one of the χ reflections (332), which is in agreement with the SEM analysis.

Cr, Mo and Si are the main elements which increase the susceptibility to σ phase precipitation. The "sigma equivalent" (σ_{eq}) is a parameter proposed by Ramirez-Londoño [2] to measure the tendency of a DSS or SDSS to σ precipitation:

$$\sigma_{eq} = X_{Cr(\delta)} + 4.5 \cdot X_{Mo(\delta)} + 1.5 \cdot X_{Si(\delta)} \quad (1)$$

where, $X_{Cr(\delta)}$, $X_{Mo(\delta)}$ and $X_{Si(\delta)}$ are the amounts of Cr, Mo and Si in the ferritic matrix.

SD-B presents slightly higher concentrations of Cr, Mo and Si than SD-A. Besides this, the amount of ferrite is lower in SD-B, which means that these elements are more concentrated in the ferrite phase of this material than in SD-A. All these facts could determine, by Eq. (1), a higher kinetics of σ precipitation in SD-B. However, it is clear that the higher grain size of SD-B exerts a stronger influence, and retards σ and other deleterious phase precipitation, as shown in Fig. 5. Since γ/δ and δ/δ grain boundaries are the main sites for χ, σ and γ_2 nucleation, the increase of grain size must naturally retards $\delta \rightarrow \chi$ and $\delta \rightarrow \sigma + \gamma_2$ reactions. This effect was more determinant to deleterious phase precipitation than the small composition differences between SD-A and SD-B.

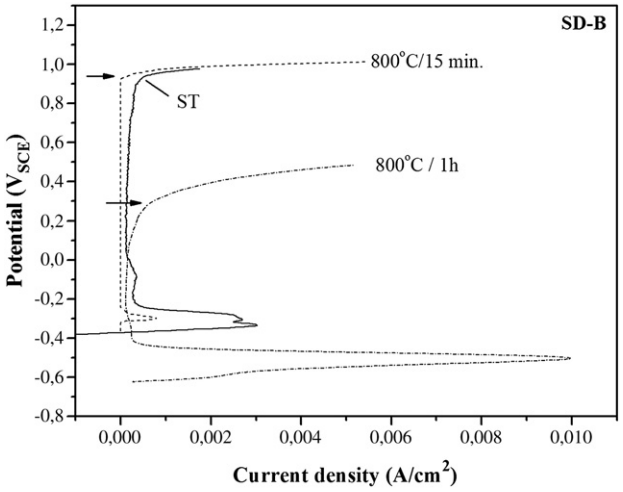

Fig. 10 – Anodic polarization curves from SD-B samples: as received (solution treated); 800 °C/60 min and 800 °C/1 h.

Table 5 – Pitting potential (E_p) values obtained in 1 M H_2SO_4 + 1 M NaCl solution

Treatment condition	Material SD-A		Material SD-B	
	% (deleterious phases)	E_p (V_{SCE})	% (deleterious phases)	E_p (V_{SCE})
As received (ST)	0	0.94	0	0.94
800 °C/60 min.	9.09	0.37	0.83	0.97
800 °C/1 h	25.99	0.06	7.75	0.35

Fig. 8 shows the hardness against aging time curves for SD-A and SD-B. The curves are very similar in shape to those of Fig. 5. However, in the initial stages of σ and other phase precipitation the hardness does not increase, and even a small softening is observed. Similar results were reported by Tavares et al. [16] and Nilsson et al. [4] for a duplex stainless steel (DSS) and a SDSS, respectively.

One of the main effects of deleterious phases in DSS and SDSS is a decrease of corrosion resistance [3,8]. Figs. 9 and 10 show the anodic polarization curves of materials SD-A and SD-B, respectively, each in the as-solution treated and 800 °C by 15 and 60 min heat treated conditions. Table 5 shows the pitting potential values obtained from the polarization tests. The coarse-grained SD-B material maintains a high E_p value after aging for 15 min at 800 °C, while the fine-grained SD-A steel presents a much lower E_p value when aged at the same condition. This is almost assuredly due to the lower percentage of deleterious phases in SD-B (0.83%) than in SD-A (9.1%). After 60 min of aging at 800 °C, however, both materials present low E_p values. Fig. 11(a) and (b) show the as-solution treated materials SD-A and SD-B after the corrosion tests. In both materials it is observed that some pits nucleated in the ferrite phase. Fig. 11(c) shows the SD-A aged at 800 °C for 15 min. A higher density of pits can be seen in the ferrite phase after this heat treatment compared to the solution treated material. Fig. 11(d) shows in detail the severe attack suffered by the ferrite phase.

4. Conclusions

The present study of the influence of grain size on the precipitation of deleterious phases in superduplex stainless steel UNS S32750 allow us to conclude:

- An increase of grain size reduces the kinetics of decomposition of ferrite into deleterious phases. Thus SD-B exhibits a lower tendency for the precipitation of deleterious phases than SD-A.
- A decrease in corrosion resistance occurs for both materials after exposure at 800 °C, although the decrease occurs in

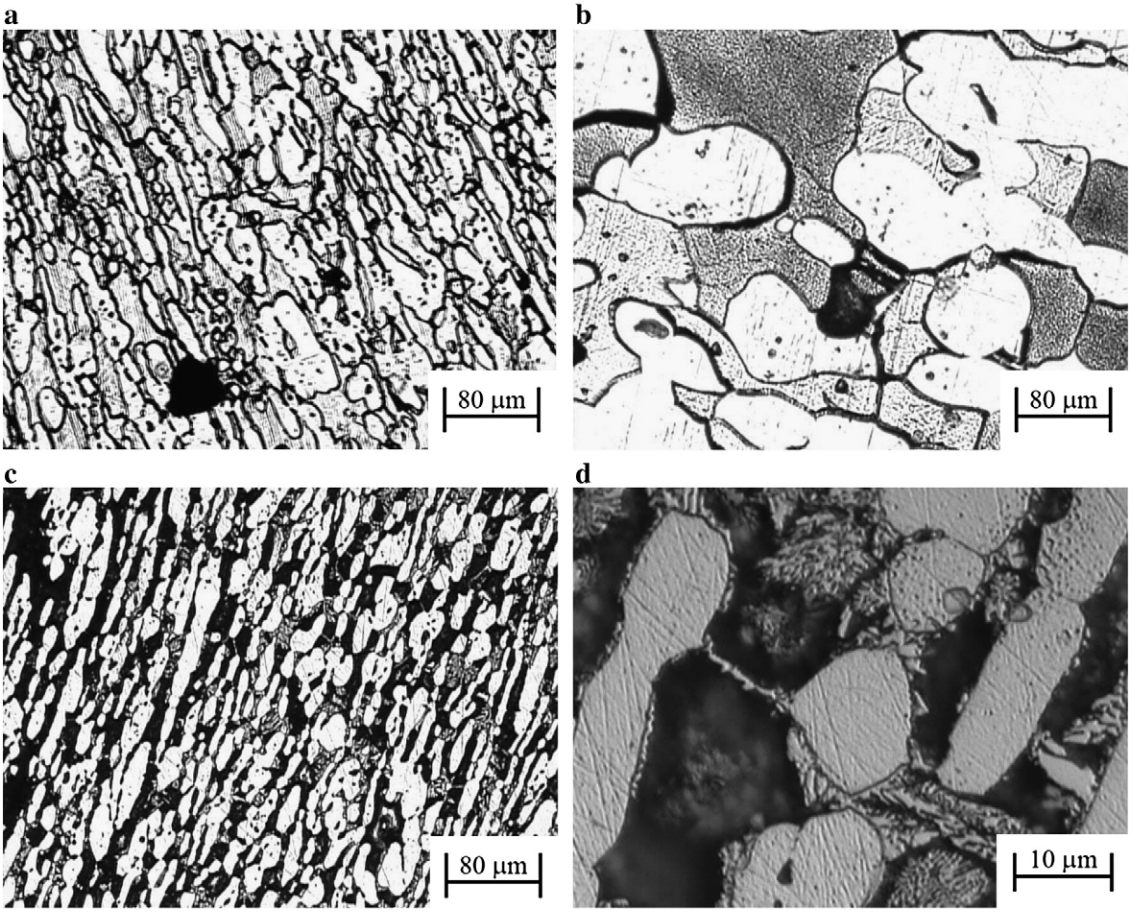

Fig. 11 – Pits and corrosion attack observed just after the anodic polarization tests: (a) SD-A-ST (as received); (b) SD-B-ST (as received); (c) and (d) SD-A-800 °C/15 min.

much shorter exposure times for SD-A than for SD-B. This reflects the lower concentration of deleterious phases in SD-B.

- The increased grain size of the SD-B material tends to mitigate the decrease in corrosion resistance after the 800 °C heat treatment.
- Pitting resulting from the anodic polarization tests was found to be concentrated in the ferrite phase, thus was more pronounced in the SD-A materials with higher ferrite fraction.

Acknowledgments

The authors acknowledge the Brazilian research agencies (CAPES, FAPERJ and CNPq) for the financial support.

REFERENCES

[1] Muthupandi V, Srinivasan PB, Seshadri SK, Sundaresan S. Effect of weld metal chemistry and heat input on the structure and properties of duplex stainless steels welds. Mat Sci Eng A 2003;A358:9–16.

[2] Ramirez Londoño, A.J., Estudo da precipitação de nitreto de cromo e fase sigma por simulação térmica da zona afetada pelo calor na soldagem multipasse de aços inoxidáveis duplex, M.Sc. Thesis 1997, University of São Paulo (USP).

[3] Lopez N, Cid M, Puiggali M. Influence of σ-phase on mechanical properties and corrosion resistance of duplex stainless steel. Corrosion Sci 1999;41:1615–31.

[4] Nilsson JO, Kangas P, Karlsson T, Wilson A. Mechanical properties, microstructural stability and kinetics of σ phase formation in 29Cr–6Ni–2Mo–0.38N superduplex stainless steel. Met Mat Trans A 2000;31A:35–45.

[5] Domínguez-Aguilar MA, Newman RC. Detection of deleterious phases in duplex stainless steel by weak galvanostatic polarization in alkaline solution. Corrosion Sci 2006;48:2560–76.

[6] Gunn RN. Duplex stainless steels—microstructure, properties and applications. Cambridge: Abington Publishing; 2003.

[7] Lee KM, Cho HS, Chjoi DC. Effect of isothermal treatment of SAF 2205 duplex stainless steel on migration of δ/γ interface boundary and growth of austenite. J Alloys Compd 1999;285:156–61.

[8] Kobayashi DY, Wolynec S. Evaluation of the low corrosion resistant phase formed during the sigma phase precipitation in duplex stainless steels. Mater Res 1999;2(4):239–47.

[9] Lippold JC, Kotecki DJ. Welding metallurgy and weldability of stainless steels. John Wiley & Sons; 2005.

[10] Nilsson JO. Super duplex stainless steels. Mater Sci Technol 1992;8:685–700.

[11] Ramirez AJ, Lippold JC, Brandi SD. The relationship between chromium nitride and secondary austenite precipitation in duplex stainless steels. Met Mat Trans A 2003;34A:1575–97.
[12] Image Tool version 3.0, University of Texas Health Science Center at San Antonio, free software. Available in http://ddsdx.uthscsa.edu/dig/itdesc.html. Access in 09.03.2007.
[13] Park CJ, Kwon HS, Lohrengel MM. Micro-electrochemical polarization study on 25% Cr duplex stainless steel. Mat Sci Eng A 2004;A 372:180–5.
[14] ASM International. Metals handbook, vol. 09. Metallography and microstructures, CD-ROM; 2004. p. 2733.
[15] Kim SB, Paik KW, Kim YG. Effect of Mo substitution by W on high temperature embrittlement characteristics in duplex stainless steels. Mat Sci Eng A 1998;A 247:67–74.
[16] Tavares SSM, Da Silva MR, Neto JM. Magnetic property changes during embrittlement of a duplex stainless steel. J Alloys Compd 2000;313:168–73.